SUPPORTING INFORMATION

Advancing Rare-Earth (4*f*) and Actinide (5*f*) Separation through Machine-Learning and Automated High-Throughput Experiments

Logan J. Augustine,[a#] Yufei Wang,[b#] Sara L. Adelman,[b*] Enrique R. Batista,[a] Stosh A. Kozimor,[b*] Danny Perez,[a*] Joshua Schrier,[c] Ping Yang[a*]

[a]Theoretical Division, Los Alamos National Lab, Los Alamos, New Mexico 87545, United States
[b]Chemistry Division, Los Alamos National Lab, Los Alamos, New Mexico 87545, United States
[c]Department of Chemistry & Biochemistry, Fordham University, The Bronx, New York 10458, United States

*Corresponding author: sadelman@lanl.gov; kozimor@lanl.gov; danny_perez@lanl.gov; pyang@lanl.gov

#Logan J. Augustine and Yufei Wang contributed equally

Number of Pages: 29
Number of Figures: 13
Number of Tables: 3

Table of Contents

S1. LANL Super Separator

Figure S1. LANL Super Separator – an automation system for high-throughput separation

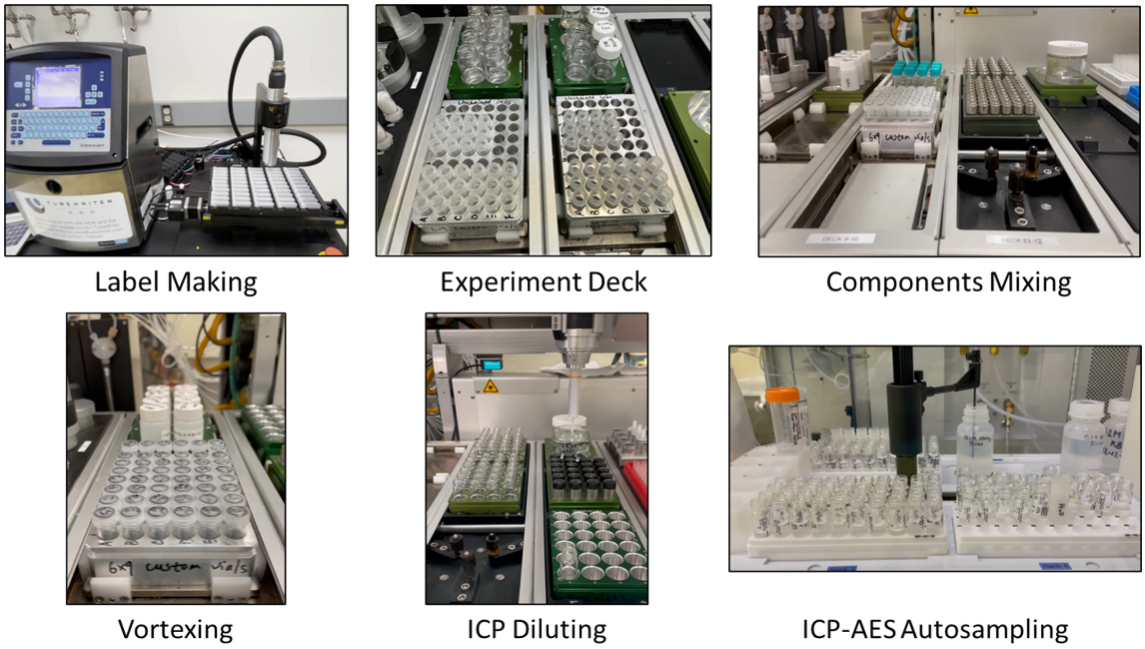

Figure S2. Step-by-step robotic executions for liquid-liquid extraction using the LANL Super Separator.

S2. *N*,*N*-dialkyl Monoamide Extractants Dataset

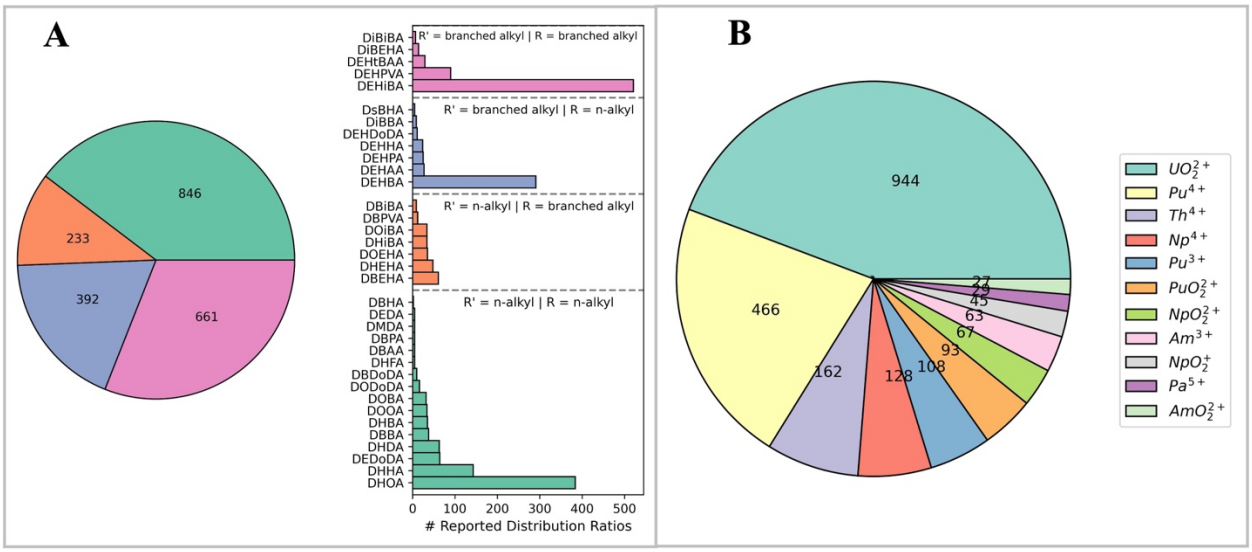

Figure S3. The *N*,*N*-dialkyl monoamide dataset broken down between (A) the different extractant types and (B) the actinide cations studied. The numbers in the pie charts represent the total number of distribution ratios reported.

Figure S3 shows a breakdown of our current *N*,*N*-dialkyl monoamide dataset which reports distribution ratios of various actinide metals focusing on the following criteria:

1. A single extractant in the organic phase
2. A single metal in the aqueous phase
3. No initial radiolytic dosage applied to either phase before extraction was performed
4. A single acid type is used in the aqueous phase (HNO_3)
5. No third-phase formation was reported upon extraction
6. The organic phase solvent was not FS-13 (CHALMEX process). This was considered as FS-13 is fairly polar compared to standard organic solvents such as n-dodecane
7. Only symmetric *N*,*N*-dialkyl monoamides were considered. Symmetric refers to when both *R'* groups bonded to the amine nitrogen are identical (see Figure 1 in main text).

This leads to a total of 2132 distribution ratios which have been extracted from previously published literature.[1-33] Overall, there are 35 unique monoamide extractants in the dataset and 11 different actinide cations. The complete dataset can be available to readers upon request. Addtionally, this dataset has also been uploaded to the Separation Archive for f-elements (SAFE) at https://safe.lanl.gov.

Table S1. Complete list of the *N*,*N* dialkyl monoamide acronyms, full names, and references which were used to for distribution ratio values in the complete monoamide dataset.

Acronym	Full Chemical Name	Reference
DEHiBA	*N*,*N*-di-2-ethylhexylisobutyramide	1, 3-9, 13, 19, 22-25, 28, 33
DEHAA	*N*,*N*-di-2-ethylhexylacetamide	2, 13, 25
DEHPA	*N*,*N*-di-2-ethylhexylpropanamide	2, 13
DEHPVA	*N*,*N*-di-2-ethylhexylpivalamide	2, 13, 19, 25
DEHBA	*N*,*N*-di-2-ethylhexylbutyramide	4, 5, 9, 19, 28, 32, 33
DHOA	*N*,*N*-dihexyloctanamide	9-12, 15, 27, 29, 31, 33
DBBA	*N*,*N*-dibutylbutyramide	11, 18
DBHA	*N*,*N*-dibutylhexanamide	11
DHHA	*N*,*N*-dihexylhexanamide	11, 14, 15
DBEHA	*N*,*N*-dibutyl-2-ethylhexanamide	11, 18, 29
DEHHA	*N*,*N*-di-2-ethylhexylhexanamide	11, 26
DHEHA	*N*,*N*-dihexyl-2-ethylhexanamide	11, 19
DOOA	*N*,*N*-dioctyloctanamide	11, 30
DHDA	*N*,*N*-dihexyldecanamide	15, 31
DHBA	*N*,*N*-dihexylbutyramide	16
DHiBA	*N*,*N*-dihexylisobutyramide	16
DOBA	*N*,*N*-dioctylbutyramide	17
DOiBA	*N*,*N*-dioctylisobutyramide	17
DHFA	*N*,*N*-dihexylformamide	18
DBAA	*N*,*N*-dibutylacetamide	18
DBPA	*N*,*N*-dibutylpropanamide	18
DBiBA	*N*,*N*-dibutylisobutyramide	18
DBPVA	*N*,*N*-dibutylpivalamide	18
DiBBA	*N*,*N*-diisobutylbutyramide	18
DiBiBA	*N*,*N*-diisobutylisobutyramide	18
DMDA	*N*,*N*-dimethyldecanamide	18
DEDA	*N*,*N*-diethyldecanamide	18
DsBHA	*N*,*N*-di-sec-butyl-hexanamide	18
DEDoDA	*N*,*N*-diethyldodecanamide	20, 21
DODoDA	*N*,*N*-dioctyldodecanamide	20
DBDoDA	N,N-dibutyldodecanamide	20
DEHDoDA	*N*,*N*-di-2-ethylhexyldodecanamide	26
DEHtBAA	*N*,*N*-di-2-ethylhexyl-tert-butyl-acetamide	26
DOEHA	*N*,*N*-dioctyl-2-ethylhexanamide	30
DiBEHA	*N*,*N*-diisobutyl-2-ethylhexanamide	30

S3. Development of the Bayesian Optimization Methodology

S3a. Data Processing for UO_2^{2+} Extraction with DEHiBA

As referenced in the main text, when considering a single metal identity with one extractant, the most studied system is UO_2^{2+} extraction with the DEHiBA ligand, representing 245 total distribution coefficients in the dataset. In this work, Gaussian Process regression was performed to predict UO_2^{2+} distribution coefficients (D_U) across five unique input parameters: (1) Extractant concentration, (2) UO_2^{2+} concentration, (3) $HNO_{3(aq)}$ concentration, (4) Total $NO_{3(aq)}^-$ concentration, and (5) Temperature. Solvent extraction in this field typically works in an acidic environment with nitric acid, $HNO_{3(aq)}$. However, since some experimental setups included inorganic nitrate salts ($LiNO_3$, $Al(NO_3)_3$, etc), we elected to treat the acid concentration and total nitrate concentration independently. Figure S4 plots the histograms for these inputs, along with the histograms on the reported D_U values.

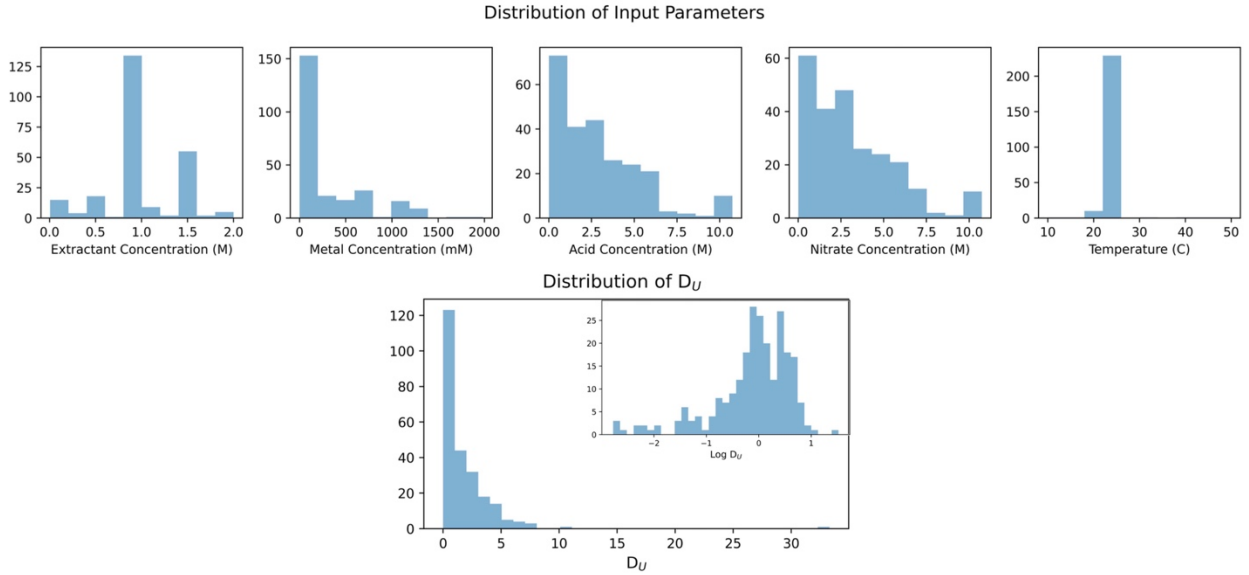

Figure S4. Histograms showing the distribution of the five unique input parameters (top) and the reported D_U values for UO_2^{2+} extraction with DEHiBA (bottom). The inset in the lower figure displays the log(D_U) values.

As depicted in Figure S4, most of the D_U values for this system are < 10, but there exists an outlier with a measured value at ~33. Therefore, this point was removed from the dataset for the kernel testing (Section S3b) and virtual experiments (Section S3c). Additionally, 61 total datapoints were missing either the initial UO_2^{2+} concentration, DEHiBA concentration, acid/nitrate concentration, and/or temperature. Therefore, the following criteria was used to handle these missing input values:

1. If no temperature was explicitly reported, then it was assumed the experiment was conducted at room temperature (25°C).
2. One study[4] did not report an initial DEHiBA concentration. But the same authors reproduce/reprint one of the figures in a later study,[23] where they report the initial DEHiBA

concentration to be 1.0 M. Therefore, this value was used for the initial DEHiBA concentration.

3. Two publications[4, 28] from the same authors report the initial [UO_2^{2+}] to be 'tracer level' with no explicit concentration value given. But later studies[2, 3] reported by the authors state UO_2^{2+} 'tracer level' concentrations to be ~0.01 mM, so this value was used. A third study[5] states "the initial metal concentration was low <100 mM" for extraction studies, while some experiments report the initial UO_2^{2+} concentration to be ≤50 mM. Therefore, a value of 50 mM was used to fill the initial UO_2^{2+}concentration for any missing values from this report.

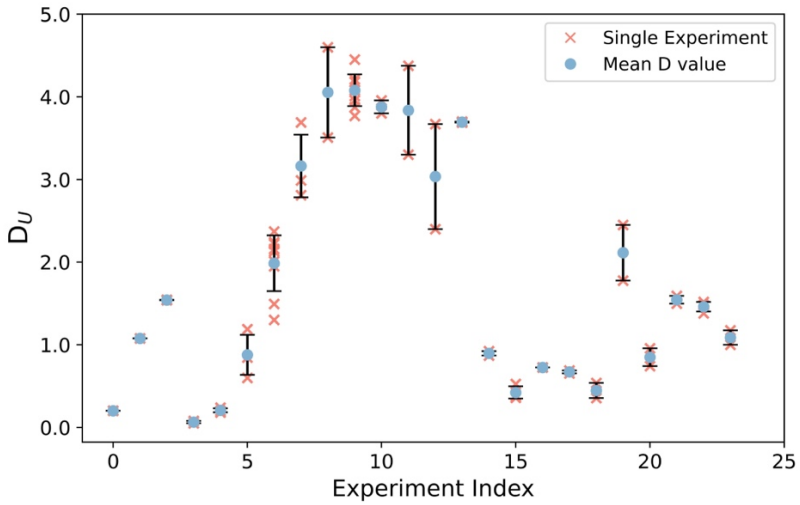

Figure S5. Duplicated inputs in the dataset examining UO_2^{2+}extraction with DEHiBA showing each reported D_U value, their mean, and standard deviation ('error bars'). The x-axis represents an arbitrary index for the duplicated experiment.

After initial handling of missing input values, 24 'duplicated' experiments were found inside the dataset. Since distribution coefficients were studied based on only five unique input values, this occurs when similar experiments are performed through (1) different labs at different times, (2) different contact (mixing) times, or (3) different organic diluents. Figure S5 shows these duplicated experiments with their measured D_U values. To keep the function-space view of Gaussian Process regression (one input:one output), we needed a way to handle the duplicated input values. One method would be to replace all duplicated inputs to a single experiment with their average D_U value. Such a technique would decrease our total dataset size from 245 to 202 total values. Since we are already dealing with a smaller size dataset, we instead chose to implement a small amount of random 'noise' into the input values, now allowing for a single input, single output of each data point. To do this, a random value was chosen from a normal Gaussian distribution with a mean equal to the original input and a 2.5% standard deviation meaning the original values were perturbed at most ~5% within a 95% confidence interval. The randomly chosen value was then used as the new input value for the experimental input space.

S3b. Gaussian Process Regression and kernel testing

In this work, regression analysis was performed using a Gaussian Process to model the experimental response surface. A Gaussian Process describes a probability distribution over all possible functions which fit a set of data points and is completely defined its mean, $\mu(\boldsymbol{x})$, and covariance (kernel) functions, $k(\boldsymbol{x}, \boldsymbol{x}')$, (Equation S1).

$$f(\boldsymbol{x}) = GP(\mu(\boldsymbol{x}), k(\boldsymbol{x}, \boldsymbol{x}')) \qquad \textbf{[S1]}$$

In practice, $\mu(\boldsymbol{x})$ is often considered to be a constant (C), while the kernel function is used to describe the relationship between adjacent points. Therefore, $k(\boldsymbol{x}, \boldsymbol{x}')$ determines most, if not all, of the generalization properties of the Gaussian Process. Real-world experiments may have measurement errors, which are modeled as a noisy response surface, $y = f(\boldsymbol{x}) + \epsilon$. Regression analysis with a Gaussian Process model in the Bayesian framework allows for the incorporation of the variance in these measurements (σ^2) into the model as shown through Equations S2-S5.

$$\begin{bmatrix} y \\ \boldsymbol{f}_* \end{bmatrix} \sim \mathcal{N}\left(C, \begin{bmatrix} \boldsymbol{K} + \sigma^2 \boldsymbol{I} & \boldsymbol{K}_* \\ \boldsymbol{K}_*^{\boldsymbol{T}} & \boldsymbol{K}_{**} \end{bmatrix}\right) \qquad \textbf{[S2]}$$

$$(\boldsymbol{f}_* | \boldsymbol{x}, y, \boldsymbol{x}_*) \sim \mathcal{N}(C + \boldsymbol{K}_*^{\boldsymbol{T}}(\boldsymbol{K} + \sigma^2 \boldsymbol{I})^{-1}(y - C), \boldsymbol{K}_{**} - \boldsymbol{K}_*^{\boldsymbol{T}}(\boldsymbol{K} + \sigma^2 \boldsymbol{I})^{-1}\boldsymbol{K}_*) \qquad \textbf{[S3]}$$

$$m(\boldsymbol{x}_*) = C + \boldsymbol{K}_*^{\boldsymbol{T}}(\boldsymbol{K} + \sigma^2 \boldsymbol{I})^{-1}(y - C) \qquad \textbf{[S4]}$$

$$\sigma^2(\boldsymbol{x}_*) = \boldsymbol{K}_{**} - \boldsymbol{K}_*^{\boldsymbol{T}}(\boldsymbol{K} + \sigma^2 \boldsymbol{I})^{-1}\boldsymbol{K}_* \qquad \textbf{[S5]}$$

Here, $\boldsymbol{x}$ and $\boldsymbol{x}_*$ represent the observed and predicted data points, respectively, and $\boldsymbol{K} = k(\boldsymbol{x}, \boldsymbol{x}')$, $\boldsymbol{K}_* = k(\boldsymbol{x}, \boldsymbol{x}_*)$, and $\boldsymbol{K}_{**} = k(\boldsymbol{x}_*, \boldsymbol{x}_*)$ are the kernel matrices formed between observed and predicted points. Lastly, Equations S4 and S5 present the predictive (posterior) mean and variance of the Gaussian Process model upon training of the kernel hyperparameters on the observed data points.

The overall efficiency of Bayesian Optimization depends on how well the Gaussian Process model can capture the true experimental response surface, and the method's decision-making strategy. In Gaussian Process modeling, the kernel function determines most, if not all, the generalization properties of the model. Therefore, the performance of the Squared-Exponential (RBF) and the Matérn classes with three unique ν values ($^5/_2, ^3/_2, ^1/_2$) (Equations S6 and S7, respectively) were examined for their prediction on D_U values from UO_2^{2+} extraction with DEHiBA. These kernels were selected as they represent the most common kernels used in Bayesian Optimization.

$$k^{RBF}(\boldsymbol{x}, \boldsymbol{x}') = \sigma^2 \exp\left(-\frac{\boldsymbol{r}^2}{2l^2}\right) + \varepsilon \qquad \textbf{[S6]}$$

$$k^{Matérn}(\boldsymbol{x}, \boldsymbol{x}') = \sigma^2 \frac{2^{(1-\nu)}}{\Gamma(\nu)}(\sqrt{2\nu}\frac{\boldsymbol{r}}{l})^{\nu} B_{\nu}\left(\sqrt{2\nu}\frac{\boldsymbol{r}}{l}\right) + \varepsilon \qquad \textbf{[S7]}$$

In Equations S6 and S7, σ^2 represents a constant scaling factor which determines the average distance away from the mean function the Gaussian Process model will deviate, while ε is used to incorporate independent and identically distributed (i.i.d) noise in the data. This was chosen as the UO_2^{2+} with DEHiBA dataset was constructed through manual data extraction of previously published literature across numerous research groups where distribution ratios were often reported without error bars. Additionally, Figure S4 shows the distribution of the five experimental parameters for the dataset where each of these parameters vary significantly in their overall magnitudes. Therefore, anisotropic versions of these kernel functions were used by redefining the input space metric with a 5×5 diagonal matrix where the inverse of effective correlation length scales (l) for each dimension defines the diagonal.[34, 35] (Equation S8) Input distances ($\boldsymbol{r}$) are then calculated on this newly defined space.

$$\boldsymbol{x_{new}} = \begin{pmatrix} \frac{1}{l_1} & 0 & 0 & 0 & 0 \\ 0 & \frac{1}{l_2} & 0 & 0 & 0 \\ 0 & 0 & \frac{1}{l_3} & 0 & 0 \\ 0 & 0 & 0 & \frac{1}{l_4} & 0 \\ 0 & 0 & 0 & 0 & \frac{1}{l_5} \end{pmatrix} \boldsymbol{x_{init}} \qquad \textbf{[S8]}$$

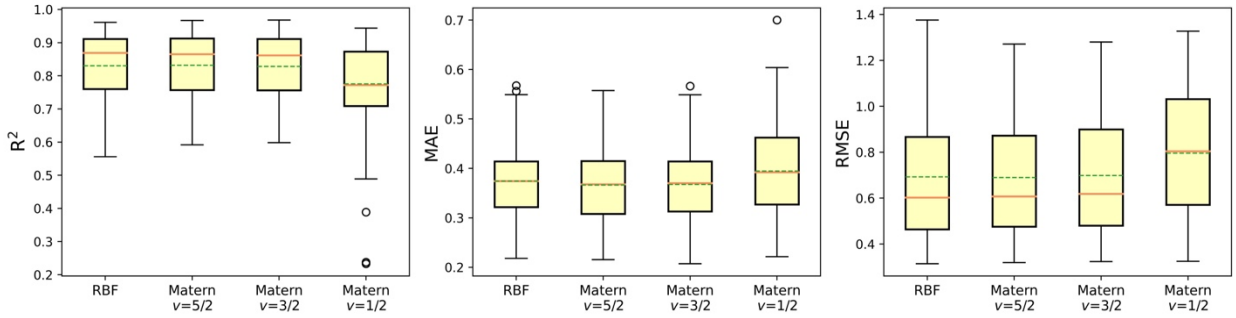

Figure S6. Performance of the RBF and Matérn kernels on the testing sets from repeated 5-fold cross-validation. Displayed are boxplots of the final R^2, mean absolute error (MAE), and root mean square error (RMSE) values between the predicted and actual D_U values in the dataset. Solid red lines represent the median of the dataset, while the dotted green lines correspond to the mean.

The overall performance of the four kernel functions was investigated through a repeated (40×) *k*-fold (*k*=5) cross-validation (Figure S6). Here, initial length-scale hyperparameters for the Gaussian Process kernel functions (Equation S6 and S7) were set the mean value of each dimension and bound by a factor of 10 above and below the minimum and maximum values of that dimension, respectively. The i.i.d noise hyperparameter was initialized at 0.001 and bound with a maximum value of 1.0 to avoid over-fitting of the noise parameter. Final kernel hyperparameters were found within these bounds by maximizing the log-marginal likelihood of data during the fitting process. Based on the resulting R^2, MAE, and RMSE values for the testing sets, the RBF and Matérn kernels

have similar performance for the when predicting D_U values for UO_2^{2+} extraction with DEHiBA. This is expected as the kernels represent very similar structure with their differences primarily being in function differentiability. Therefore, to compare this factor further, selected regions of the dataset were examined to investigate how each Gaussian Process model performs in predicting D_U when varying each input parameter. As depicted in Figure S7, the RBF kernel results in a smooth function prediction as the kernel is infinitely differentiable. When transitioning to the Matérn kernel class, these functions become rougher, as they correspond to twice differentiable ($\nu=5/2$), once differentiable ($\nu=3/2$), and an absolute exponential kernel ($\nu=1/2$). As the anisotropic RBF kernel appears to interpolate between reported D_U values the best, this kernel function was elected to for further Bayesian Optimization development (Section S2c) involving this dataset. However, based on the results in Figure S6 and Figure S7, similar outcomes may be expected between the RBF and Matérn kernels.

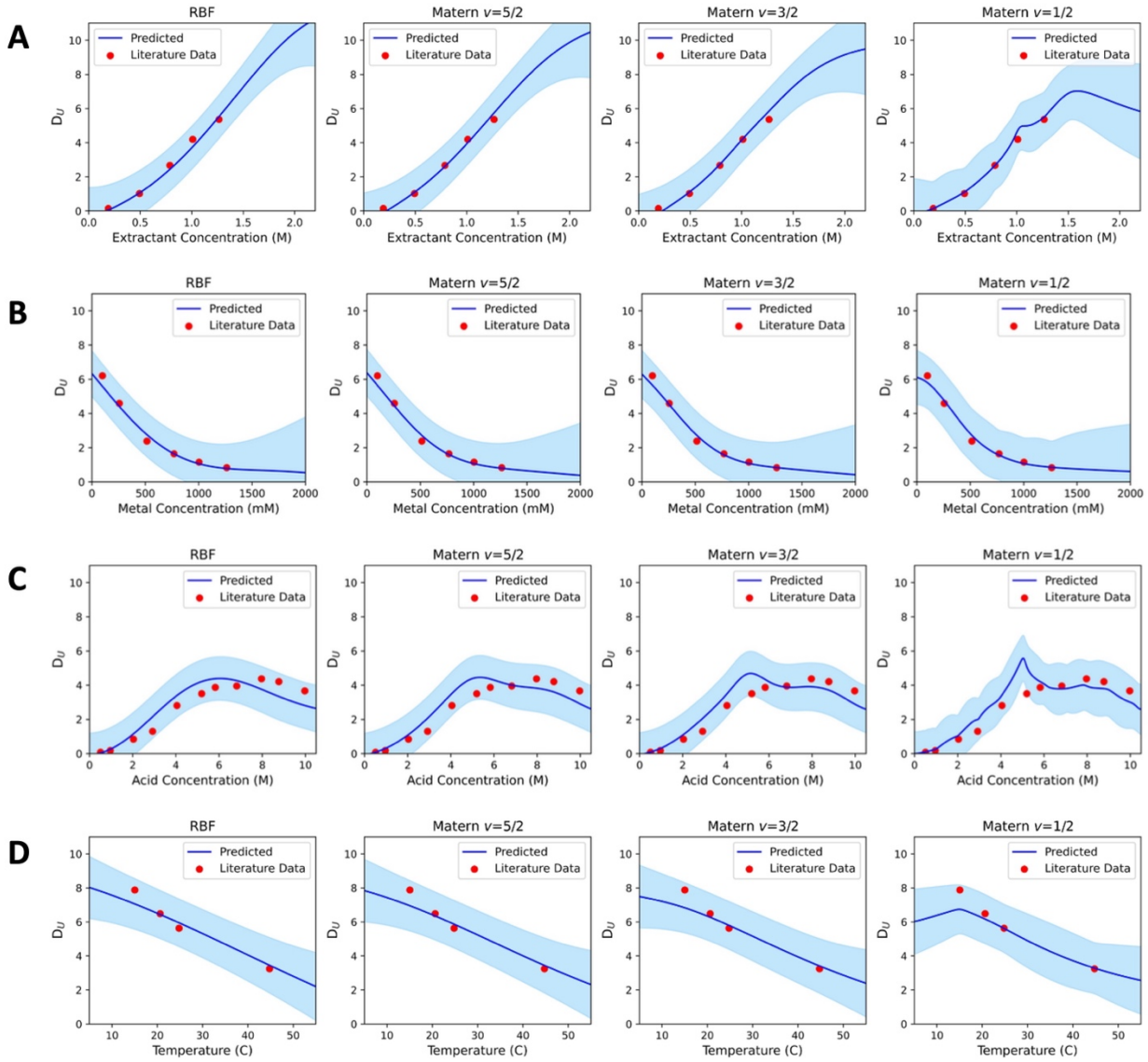

Figure S7. Performance of the various kernel functions with varying (A) Extractant Concentration, (B) Metal Concentration, (C) Acid Concentration, and (D) Temperature. Here, the Gaussian Process model was trained on the whole dataset before prediction on specified regions with a single varied input parameter. Shaded regions represent the 95% confidence region for the Gaussian Process mean posterior prediction.

S3c. Virtual Optimization Campaigns for UO_2^{2+} Extraction by DEHiBA

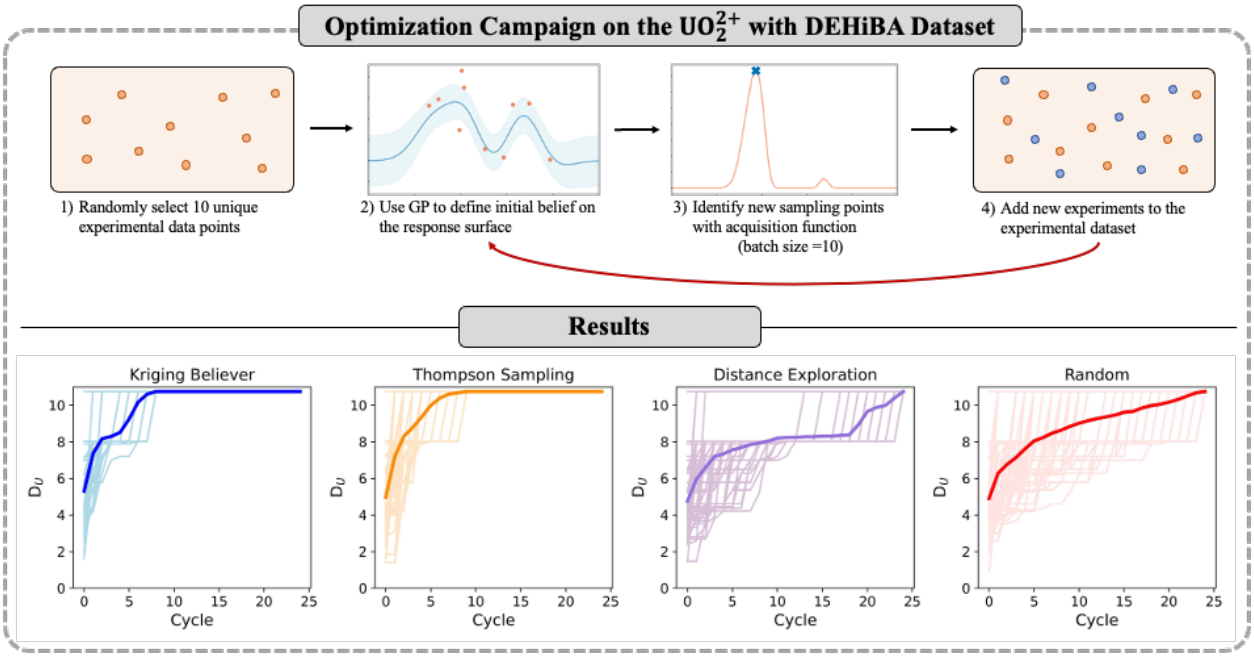

Figure S8. (Top) Representative schematic of the virtual Bayesian Optimization campaigns performed for the extraction of UO_2^{2+} by DEHiBA. (Bottom) Results from these campaigns using various acquisition functions. Lighter lines correspond to one of the 75 virtual campaigns while the dark bolded lines correspond to the average of these tests.

To further develop the Bayesian Optimization methodology for our work, the performance of various acquisition functions was examined through virtual optimization campaigns of UO_2^{2+} extraction by DEHiBA (Figure S8). Three acquisition function types were evaluated based on their selection criteria: (1) Kriging Believer[36-38], (2) Thompson Sampling[39, 40], and (3) Distance Exploration[41], and compared to randomly selecting experiments to generate a new batch. Pseudocodes for each acquisition function are provided in Section S4. It is observed both the Kriging Believer and Thompson Sampling methods, on average, find the maximum D_U value after the ~8th cycle. This corresponds to needing to perform (at most) 90 total experiments or sampling ~37% of the experimental space (244 total experiments) compared to the Distance Exploration and random selection methods, which both needed to sample almost the entire experimental space before finding the maximum D_U value.

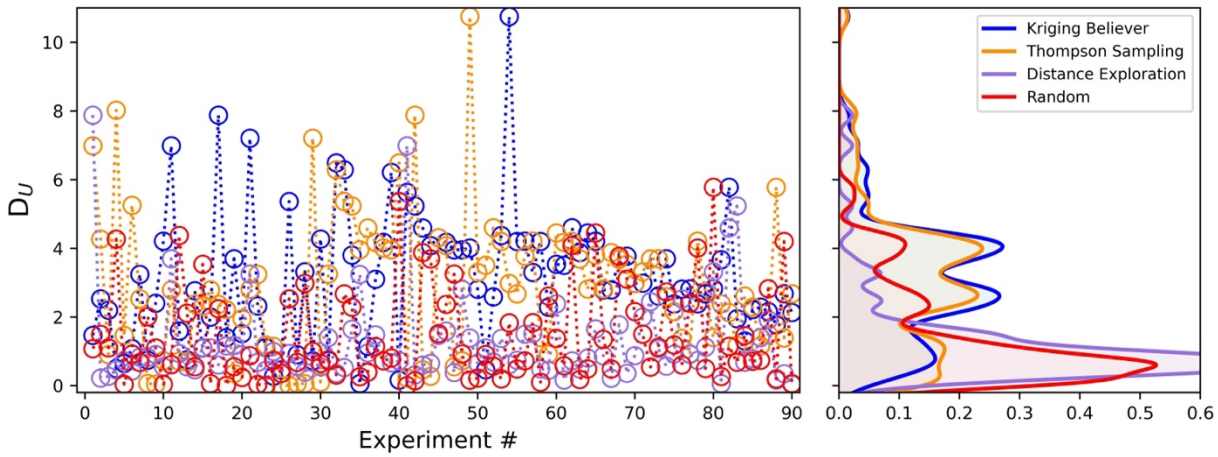

Figure S9. (Left) Measured D_U of the first 90 selected experiments from a selected toy experiment on the U(VI)/D2EHiBA dataset. (Right) Density plot of the measured D_U values from these first 90 selected experiments.

To further show the utility of Bayesian Optimization for actinide separations, the D_U values of the first 90 selected conditions from a single virtual optimization campaign is presented in Figure S9. The density plots indicate that the Kriging Believer and Thompson Sampling methodologies prioritize sampling experiments with D_U values > 2.0, whereas the Distance Explorer and random sampling methods favor sampling of D_U values < 2.0 during this same time frame. These results follow what has previously been observed in chemical reaction optimization.[42]

Due to these encouraging results, this Bayesian Optimization methodology using the anisotropic RBF kernel for Gaussian Process modeling and the Kriging Believer acquisition function was applied to optimize solvent extraction of the Th^{4+} cation with DEHBA. Here, we note that each unique solvent extraction experiment of Th^{4+} with DEHBA was performed in triplicate. Therefore, the Gaussian Process model was fit to the experimentally measured mean D_{Th} value, while the measured variance was used for input noise.[34] This removed the need for the additional i.i.d noise kernel used in Equation S6.

S4. Acquisition Functions

Pseudocode for the Kriging Believer, Thompson Sampling, and Pure Exploration acquisition are given below.

Kriging Believer Algorithm

Inputs

D: observed dataset
$cand$: sampling candidates
b: batch size
EI: Expected Improvement acquisition function
$NewBatch$: holds newly suggested experiments

Batch Selection

$Model = GaussianProcess(D)$
$Model.optimize()$
$x_i = argmax(EI(cand))$
$y_i = model.predict(cand)[x_i]$
$NewBatch.append(x_i)$
$D.append((x_i, y_i))$
$while\ size(NewBatch) < b$:
    $NewModel = GaussianProcess(D)$ // Use original model's hyperparameters
    $NewModel.optimize()$ // Keep hyperparameters fixed. Updates the posterior distribution of the Gaussian Process
    $x_i = argmax(EI(cand))$
    $y_i = model.predict(cand)[x_i]$
    $NewBatch.append(x_i)$
    $D.append((x_i, y_i))$

Thompson Sampling Algorithm

Inputs

D: observed dataset
$cand$: sampling candidates
b: batch size
$NewBatch$: holds newly suggested experiments

Batch Selection

$Model = GaussianProcess(D)$
$Model.optimize()$
$while\ size(NewBatch) < b$:
    $sample = Model.sample(cand)$ // Randomly draw a sample from the Gaussian Process posterior evaluated at the candidate points
    $x_i = argmax(sample)$
    $NewBatch.append(x_i)$

Pure Explorer Algorithm

Inputs

D: observed dataset
$cand$: sampling candidates
b: batch size
EI: Expected Improvement acquisition function
$NewBatch$: holds newly suggested experiments

Batch Selection

$Model = GaussianProcess(D)$
$Model.optimize()$
$x_i = argmax(EI(cand))$
$NewBatch.append(x_i)$ // First point of the batch comes from the max EI value
$distances = \sqrt{(x_i - x_j)^2}\ for\ j\ in\ cand$
$NewBatch.append(argsort(distances,\ order = descending)[:(b-1)])$ // Fill the rest of the batch with the furthest points away from the EI max value

S5. Bayesian Optimization for $Th^{4+}_{(aq)}$ Extraction with DEHBA containing an Anomalous Experiment

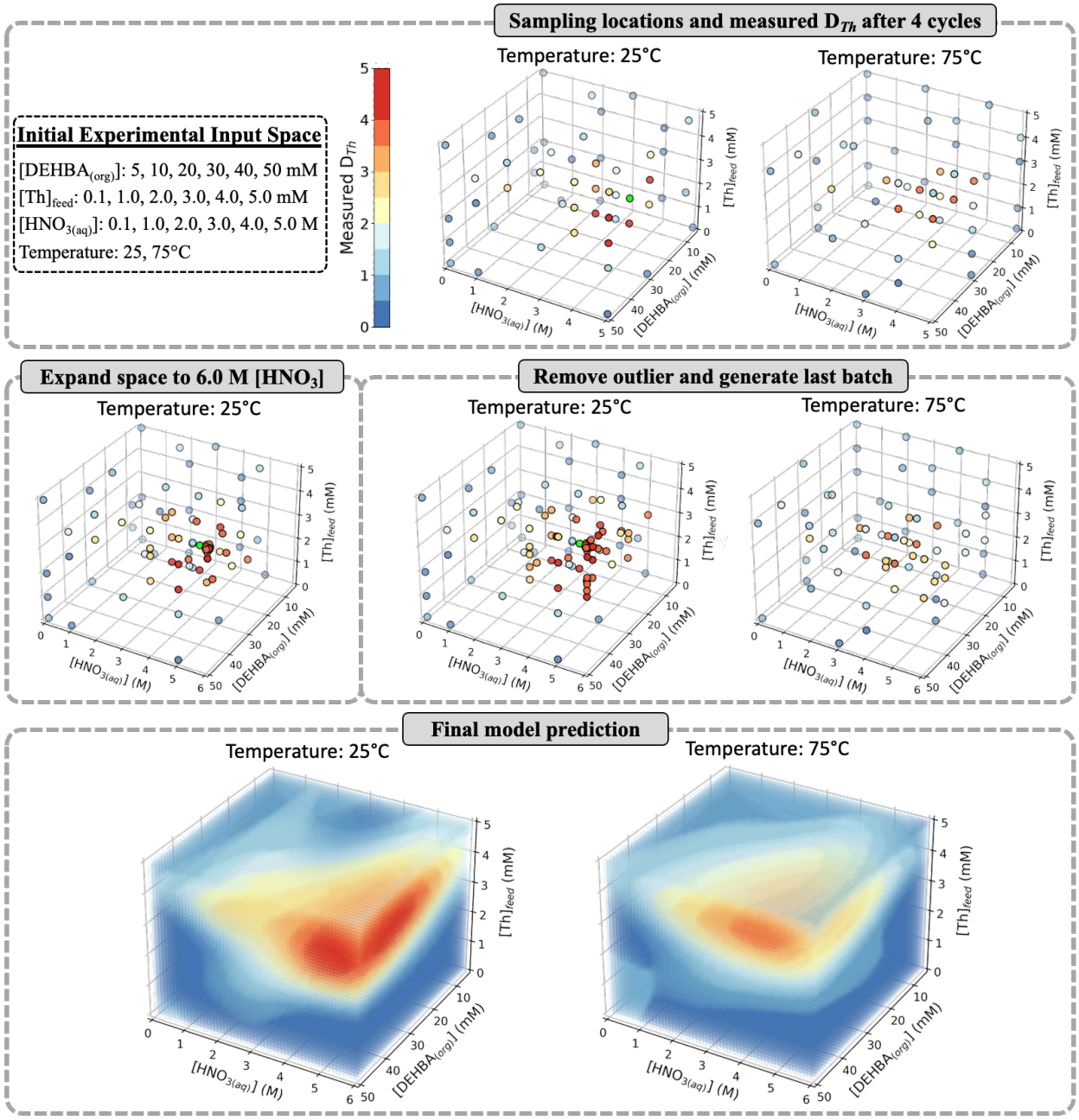

Figure S10. (Top) Sampling locations and measured D_{Th} values across the four-dimensional experimental input space after four Bayesian Optimization cycles on the extraction of $Th^{4+}_{(aq)}$ by DEHBA in 20v% TBP/*n*-dodecane organic phase. (Middle) Sampling and measured D_{Th} values after expansion of the input space into 6.0 M [$HNO_{3(aq)}$]. In the top and middle sections, the location of the anomalous experiment with $D_{Th} = 6.58 \pm 0.05$ is shown in green. (Bottom) Heat map showing the predicted D_{Th} values from the final Gaussian Process model after all six Bayesian Optimization cycles were complete.

Figure S10 provides the initial four-dimensional experimental input space which was generated to evaluate the extraction of $Th^{4+}_{(aq)}$ from aqueous nitric acid solutions into an organic solution composed of DEHBA dissolved in 20v% TBP/*n*-dodecane. After four experimental cycles, initially a maximum D_{Th} value of 6.58 ± 0.05 was observed using the experimental conditions of $[Th^{4+}_{(aq)}]$ = 4.0 mM, $[HNO_{3(aq)}]$ = 5.0 M, $[DEHBA_{(org)}]$ = 40 mM, and temperature = 25°C. A fifth batch of predicted experimental conditions was generated from the measurements which resulted in a single a single D_{Th} prediction of 4.50 while all other values were < 2.80. Since none of these conditions were expected to improve upon our current maximum D_{Th} value (6.58 ± 0.05), and the Gaussian Process model showed good prediction inside the experimental space (Cycle 4, Figure S11a), we explored conditions beyond the initial experimental bounds in an effort to exceed our currently highest measured D_{Th} value. Here, the Gaussian Process model predicted that nitric acid concentrations higher than 5.0 M could yield even higher D_{Th} values, therefore, a new experimental batch using a tighter grid centered around the 6.58 ± 0.05 value and expanding out 6.0 M $[HNO_{3(aq)}]$ was generated. Upon measurement of the new batch, no D_{Th} values were observed > 4.03, (Figure S10) and there was a drastic decrease in the model performance (Cycle 5, Figure S11a). As many of these measurements were performed at experimental conditions similar to those that achieved the 6.58 ± 0.05 value, it was suspected that this may have resulted from an anomalous experiment and was contaminating the Gaussian Process model. To investigate this further, the 6.58 experiment was removed from the dataset and Gaussian Process model retraining was performed at each cycle again. This resulted in improved predictions in Cycles 4-5 (Figure S11a vs Figure S11b), strongly suggesting an experimental anomaly, likely arising from an error in the accuracy in the robotic liquid dispensing. With the 6.58 datapoint removed from the dataset, one final experimental batch was generated and run to verify good model performance (Cycle 6, Figure S9b) and convergence of the D_{Th} values inside the newly expanded experimental space with maxima ~4.0.

We do note that the MAE values for the Gaussian Process predictions increase Cycles 5 and 6 compared to Cycle 4, even with the anomalous experiment removed. These cycles represent the point in our experimental work where the experimental space was expanded beyond the initial boundary of 5.0 M HNO_3. Gaussian Processes are well-known for their poor extrapolation behavior, and standard kernel functions like the RBF kernel used in this work will always extrapolate back to their prior mean function as they extend beyond observed data points. Of the 72 unique experiments performed in cycles 5 and 6, 53 were located outside the original bounds of our experimental space. Therefore, we believe the drop in performance is due to the poor extrapolation behavior of the model.

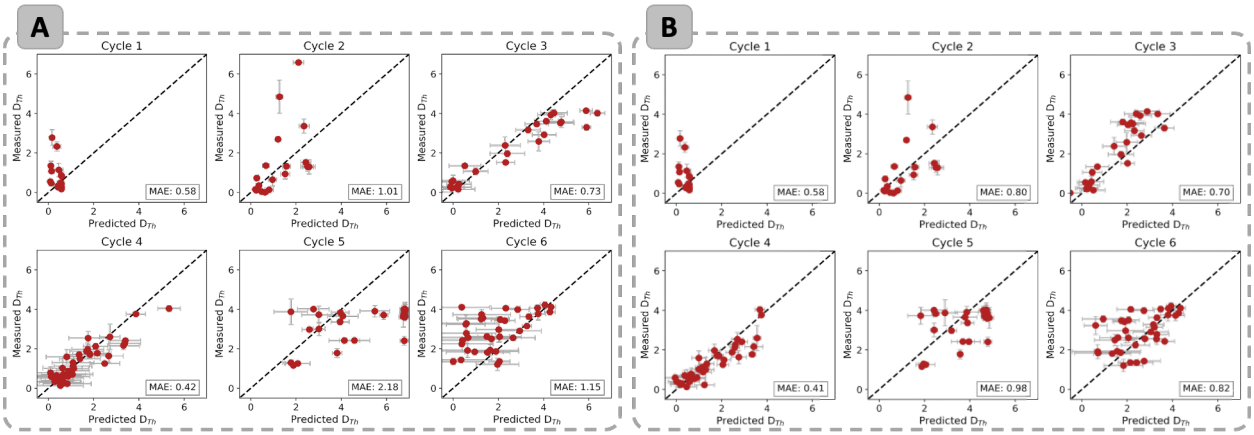

Figure S11. (A) Measured vs. predicted D_{Th} values for the six experimental cycles of Bayesian Optimization for $Th^{4+}_{(aq)}$ extraction by DEHBA. Here, the anomalous experiment is shown in Cycle 2. (B) Measured vs. predicted D_{Th} values for the six experimental cycles after removing the anomalous experiment and retraining the Gaussian Process model at each cycle. Error bars represent a single standard deviation from the predicted and measured values.

S6. Comparison of Different Experimental Optimization Techniques

To compare the efficiency of the Bayesian Optimization approach in identifying the optimal separation conditions, different experimental sampling techniques were explored for reaction optimization. Here, the final Gaussian Process model predictions (Figure 4 in main text) were used as a surrogate response surface of our initial experimental space. Initially, we examined the performance of one-factor-at-a-time (OFAT) sampling, and random sampling compared to Bayesian Optimization. To simulate OFAT sampling of the experimental space, a random variable was initially chosen as the independent variable while the remaining three variables were held constant (initial values were also randomly chosen). After sampling through the independent variable's values, the maximum location of the 'measured' D_{Th} was identified and held constant while sampling through the next variable. This process was repeated until all four variables were sampled. An example of this approach, representing a total of 20 experiments performed in a single OFAT cycle is shown in Table S2. If the maximum D_{Th} was not identified, then the OFAT cycles were repeated while using checks to make sure similar independent/constant variable combinations were not performed more than once.

Table S2. Example sampling locations and measured D_{Th} values for one-factor-at-a-time (OFAT) experiment.

Exp ID	$[Th]_{feed}$	$[HNO_{3(aq)}]$ (M)	$[DEHBA_{(org)}]$ (mM)	Temperature (°C)	D_{Th}
1	2.00	0.10	10.00	25.00	0.17
2	2.00	1.00	10.00	25.00	0.11
3	2.00	2.00	10.00	25.00	0.29
4	2.00	3.00	10.00	25.00	0.60
5	2.00	4.00	10.00	25.00	0.74
6	2.00	5.00	10.00	25.00	0.55
7	2.00	4.00	5.00	25.00	0.57
8	2.00	4.00	10.00	25.00	0.74
9	2.00	4.00	20.00	25.00	1.09
10	2.00	4.00	30.00	25.00	1.38
11	2.00	4.00	40.00	25.00	1.51
12	2.00	4.00	50.00	25.00	1.44
13	0.10	4.00	40.00	25.00	0.31
14	1.00	4.00	40.00	25.00	0.18
15	2.00	4.00	40.00	25.00	1.51
16	3.00	4.00	40.00	25.00	2.94
17	4.00	4.00	40.00	25.00	3.63
18	5.00	4.00	40.00	25.00	2.64
19	4.00	4.00	40.00	25.00	3.63
20	4.00	4.00	40.00	75.00	3.78

As a single OFAT cycle refers to a total of 20 experiments, virtual Bayesian Optimization and random sampling campaigns were examined using a batch size of 20 at cycle. The virtual OFAT, Bayesian Optimization, and random sampling optimization campaigns were then performed a total of 75 times to examine, on average, how quickly the optimal experimental conditions could be identified. This was needed as the initial batch for each virtual campaign was randomly generated. Results comparing each of the approaches are provided in Figure S12.

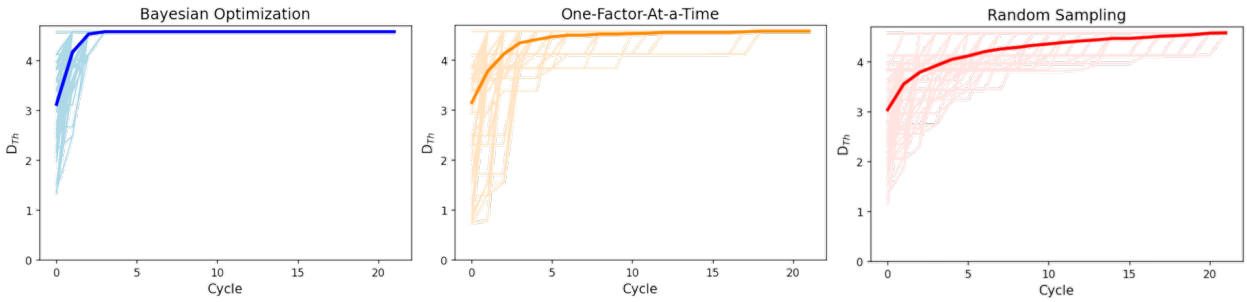

Figure S12. Virtual optimization campaigns using Bayesian Optimization, One-Factor-At-a-Time, and Random sampling techniques. On average, optimization was found after 3, 6, and 11 experimental cycles for Bayesian Optimization, OFAT, and Random sampling, respectively.

Lastly, we examined the performance of response surface modeling using a Design of Experiments full-factorial sampling technique. Here, different factorial levels (2-4) were used to determine the sampling locations along the experimental space, while the results were fit using both quadratic and cubic polynomial functions. During the fitting process, all main effect terms (the input variables) were kept, while interaction terms which contained insignificant p-values (>0.10) were removed from the final equation. Figure S13 shows the final predictions from the fitted polynomial functions compared the actual D_{Th} on the surrogate response surface. As expected, increasing the factorial level and degree of the polynomial function improved the fitting, but even with a four-level factorial sampling (256 experiments), the location of highest D_{Th} value predicted by a cubic polynomial is not the same as the optimal D_{Th} value on the surrogate response surface. Such an effect shows the advantage of using a nonparametric modeling technique (such as a Gaussian Process) for modeling experimental response surfaces and applying those results to efficiently identifying the optimal conditions.

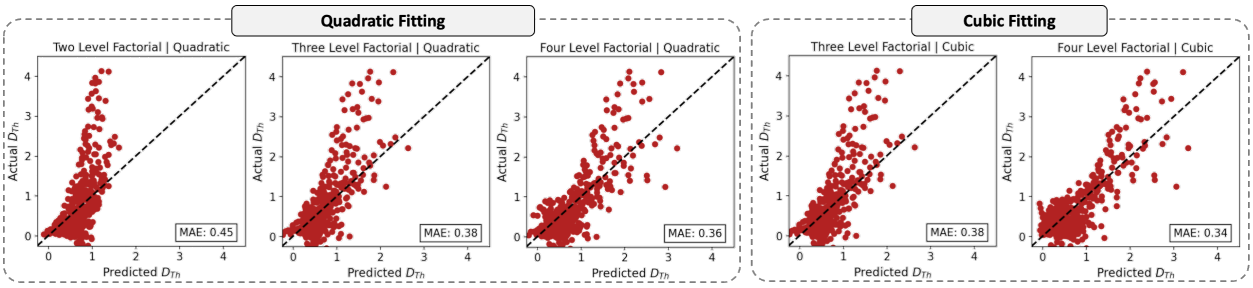

Figure S13. Actual vs. Predicted D_{Th} values from the fitted polynomials based on full factorial sampling.

S7. Measured D_{Th} Values at Various Conditions

Table S3. Complete list of the unique conditions, measured, and predicted D_{Th} values for the $Th^{4+}_{(aq)}$ liquid-liquid extraction experiments

Exp ID	[Th(IV)] (mM)	[HNO_3] (M)	[DEHBA] (mM)	Temperature (°C)	Exp D avg	Exp σ	ML Pred D	ML Pred σ	ΔD	
1	0.10	0.10	5.00	25.00	0.71	0.31	***	***	***	
2	0.10	5.00	5.00	25.00	0.08	0.04	***	***	***	
3	0.10	0.10	30.00	25.00	0.70	0.74	***	***	***	
4	0.10	5.00	30.00	25.00	0.10	0.04	***	***	***	
5	13.00	0.10	5.00	25.00	0.68	0.93	***	***	***	
6	41.00	5.00	5.00	25.00	0.42	0.18	***	***	***	
7	12.00	0.10	30.00	25.00	0.79	0.45	***	***	***	
8	78.00	5.00	30.00	25.00	2.68	1.39	***	***	***	
9	0.10	0.10	5.00	75.00	0.57	0.53	***	***	***	
10	0.10	5.00	5.00	75.00	0.04	0.01	***	***	***	
11	0.10	0.10	30.00	75.00	0.24	0.29	***	***	***	
12	0.10	5.00	30.00	75.00	0.09	0.02	***	***	***	
13	5.00	0.10	5.00	75.00	0.79	0.20	***	***	***	
14	16.00	5.00	5.00	75.00	0.91	1.24	***	***	***	
15	5.00	0.10	30.00	75.00	0.54	0.21	***	***	***	
16	16.00	5.00	30.00	75.00	3.29	2.64	***	***	***	**Cycle 0**
17	5.00	5.00	50.00	25.00	2.78	0.39	0.16	0.04	2.62	
18	5.00	0.10	50.00	25.00	0.83	0.22	0.59	0.12	0.24	
19	0.10	0.10	50.00	25.00	0.86	0.25	0.57	0.12	0.30	
20	5.00	2.00	10.00	25.00	1.14	0.34	0.46	0.17	0.68	
21	2.00	0.10	5.00	25.00	0.44	0.01	0.57	0.11	0.13	
22	3.00	1.00	50.00	25.00	0.34	0.08	0.55	0.14	0.21	
23	0.10	1.00	10.00	25.00	0.33	0.14	0.52	0.14	0.19	
24	0.10	1.00	50.00	25.00	0.48	0.15	0.53	0.15	0.05	
25	0.10	2.00	5.00	25.00	0.27	0.12	0.42	0.18	0.16	
26	0.10	5.00	50.00	25.00	0.47	0.14	0.12	0.03	0.35	
27	2.00	0.10	10.00	25.00	0.17	0.01	0.57	0.11	0.40	
28	2.00	0.10	50.00	25.00	0.28	0.15	0.57	0.12	0.29	
29	2.00	2.00	5.00	25.00	0.35	0.04	0.44	0.17	0.09	
30	2.00	5.00	10.00	25.00	0.55	0.12	0.08	0.02	0.47	
31	2.00	5.00	50.00	25.00	1.08	0.13	0.14	0.04	0.94	
32	3.00	2.00	20.00	25.00	0.36	0.05	0.45	0.17	0.09	
33	5.00	3.00	50.00	25.00	2.33	0.24	0.37	0.17	1.95	
34	5.00	5.00	10.00	25.00	1.35	0.24	0.10	0.03	1.24	**Cycle 1**
35	5.00	5.00	50.00	75.00	1.30	0.36	2.58	0.27	1.28	
36	5.00	5.00	40.00	75.00	1.30	0.24	2.50	0.28	1.20	
37	5.00	4.00	50.00	75.00	1.53	0.05	2.43	0.22	0.90	**Cycle 2**

38	5.00	4.00	40.00	25.00	3.36	0.36	2.35	0.22	1.01	
39*	**4.00**	**5.00**	**40.00**	**25.00**	**6.58**	**0.05**	**2.11**	**0.23**	**4.48**	
40	5.00	3.00	20.00	75.00	0.94	0.25	1.52	0.20	0.58	
41	3.00	5.00	5.00	75.00	0.14	0.04	0.81	0.18	0.67	
42	5.00	2.00	40.00	75.00	1.33	0.11	1.58	0.18	0.25	
43	2.00	3.00	50.00	25.00	1.36	0.09	0.67	0.15	0.69	
44	4.00	0.10	5.00	75.00	0.01	0.00	0.63	0.15	0.62	
45	4.00	3.00	5.00	75.00	0.65	0.32	0.96	0.18	0.31	
46	1.00	0.10	50.00	25.00	0.35	0.06	0.36	0.12	0.01	
47	4.00	2.00	50.00	25.00	2.69	0.08	1.20	0.12	1.49	
48	3.00	4.00	40.00	25.00	4.85	0.84	1.27	0.15	3.57	
49	1.00	2.00	5.00	75.00	0.11	0.02	0.24	0.09	0.13	
50	1.00	0.10	10.00	25.00	0.73	0.15	0.26	0.08	0.47	
51	1.00	5.00	5.00	75.00	0.16	0.02	0.21	0.08	0.05	
52	3.00	0.10	5.00	75.00	0.04	0.00	0.48	0.11	0.44	
53	4.00	5.00	50.00	25.00	4.02	0.14	6.38	0.33	2.36	
54	4.00	5.00	50.00	75.00	3.52	0.14	4.75	0.61	1.23	
55	3.00	5.00	50.00	25.00	4.03	0.18	4.46	0.59	0.43	
56	4.00	4.00	40.00	25.00	3.30	0.15	5.89	0.19	2.59	
57	4.00	5.00	30.00	25.00	4.15	0.04	5.88	0.28	1.73	
58	3.00	3.00	50.00	75.00	1.96	0.16	2.39	0.77	0.43	
59	4.00	5.00	30.00	75.00	3.61	0.15	4.11	0.53	0.50	
60	3.00	5.00	30.00	25.00	2.58	0.49	3.79	0.48	1.20	
61	1.00	4.00	50.00	75.00	0.16	0.05	0.22	0.74	0.07	
62	4.00	0.10	50.00	75.00	0.60	0.28	-0.01	0.73	0.60	
63	2.00	4.00	30.00	75.00	1.35	0.12	0.51	0.70	0.84	
64	4.00	0.10	30.00	25.00	0.28	0.04	-0.12	0.61	0.40	
65	4.00	3.00	40.00	75.00	3.17	0.17	3.31	0.55	0.14	
66	0.10	3.00	50.00	75.00	0.43	0.08	0.26	0.55	0.17	
67	4.00	5.00	5.00	75.00	1.06	0.17	1.00	0.55	0.07	
68	3.00	0.10	30.00	75.00	0.02	0.02	-0.63	0.62	0.65	
69	3.00	4.00	50.00	25.00	2.93	0.10	4.02	0.53	1.10	
70	3.00	4.00	30.00	75.00	2.38	0.43	2.30	0.67	0.08	
71	2.00	2.00	30.00	75.00	0.26	0.08	0.15	0.66	0.11	
72	2.00	4.00	5.00	75.00	0.55	0.05	-0.06	0.48	0.61	
73	4.00	4.00	50.00	75.00	3.93	0.24	4.32	0.58	0.39	
74	3.00	3.00	5.00	75.00	0.22	0.06	-0.05	0.38	0.27	
75	4.00	2.00	30.00	25.00	1.52	0.08	2.32	0.40	0.80	
76	4.00	4.00	30.00	75.00	3.46	0.05	3.69	0.52	0.23	
77	4.00	5.00	40.00	75.00	3.57	0.28	4.78	0.53	1.21	
78	3.00	5.00	40.00	25.00	4.04	0.15	5.33	0.49	1.29	
79	3.00	5.00	50.00	75.00	2.16	0.20	3.32	0.70	1.15	
80	3.00	4.00	40.00	75.00	2.41	0.11	3.40	0.67	0.99	

Cycle 3

Cycle 4

81	4.00	4.00	5.00	25.00	0.23	0.03	0.83	1.04	0.60	
82	2.00	4.00	30.00	25.00	1.30	0.10	1.09	0.92	0.21	
83	0.10	0.10	50.00	75.00	0.65	0.36	0.36	1.09	0.29	
84	5.00	3.00	30.00	25.00	1.50	0.04	1.39	0.90	0.11	
85	4.00	2.00	50.00	75.00	2.54	0.34	1.75	0.85	0.78	
86	3.00	5.00	30.00	75.00	1.64	0.33	2.66	0.64	1.03	
87	5.00	4.00	5.00	75.00	0.71	0.26	1.06	0.90	0.35	
88	5.00	2.00	5.00	75.00	0.69	0.15	0.66	0.97	0.03	
89	5.00	2.00	50.00	25.00	1.26	0.04	2.49	0.67	1.23	
90	5.00	1.00	30.00	25.00	0.88	0.07	0.89	0.91	0.02	
91	3.00	3.00	40.00	25.00	1.71	0.16	1.84	0.77	0.13	
92	1.00	4.00	5.00	25.00	0.31	0.04	0.52	0.93	0.21	
93	2.00	2.00	50.00	75.00	0.79	0.30	0.09	0.98	0.70	
94	4.00	2.00	5.00	25.00	0.24	0.01	0.65	0.89	0.41	
95	5.00	3.00	5.00	25.00	0.60	0.08	0.87	0.95	0.27	
96	5.00	1.00	50.00	75.00	1.59	0.38	0.81	0.92	0.78	
97	4.00	1.00	30.00	75.00	1.02	0.56	0.62	0.86	0.40	
98	3.00	3.00	30.00	75.00	1.97	0.32	1.73	0.71	0.24	
99	2.00	1.00	5.00	75.00	0.34	0.13	0.28	0.82	0.06	
100	3.00	4.00	30.00	25.00	1.88	0.04	1.68	0.74	0.20	
101	4.00	4.00	40.00	75.00	3.76	0.09	3.87	0.42	0.10	
102	1.00	0.10	30.00	75.00	0.59	0.17	0.13	0.79	0.46	
103	1.00	0.10	5.00	75.00	0.39	0.06	0.63	0.77	0.24	
104	5.00	4.00	50.00	25.00	2.13	0.16	2.08	0.54	0.04	
105	2.00	5.00	30.00	75.00	1.12	0.05	1.09	0.84	0.03	
106	3.00	4.00	5.00	25.00	0.13	0.09	0.53	1.02	0.39	
107	4.00	1.00	50.00	25.00	1.70	0.15	1.36	0.56	0.35	
108	2.00	4.00	50.00	75.00	1.00	0.63	1.12	0.67	0.12	
109	4.00	4.00	50.00	25.00	2.60	0.64	2.72	0.46	0.12	
110	4.00	4.00	30.00	25.00	1.77	0.06	2.16	0.61	0.39	
111	1.00	5.00	30.00	75.00	0.40	0.27	0.35	0.68	0.05	
112	5.00	0.10	5.00	25.00	0.54	0.03	0.47	1.08	0.07	
113	5.00	5.00	30.00	25.00	2.27	0.05	3.37	0.71	1.10	
114	4.00	5.30	40.00	25.00	3.94	0.30	6.82	0.18	2.88	**Cycle 5**
115	3.85	5.30	40.50	25.00	3.62	0.52	6.74	0.20	3.12	
116	3.95	5.30	39.00	25.00	2.41	0.22	6.79	0.18	4.38	
117	4.00	5.25	40.00	25.00	3.69	0.20	6.81	0.15	3.12	
118	4.00	5.35	40.00	25.00	3.97	0.39	6.81	0.21	2.84	
119	4.10	5.30	39.50	25.00	4.00	0.21	6.77	0.19	2.77	
120	4.00	5.25	40.50	25.00	3.92	0.22	6.80	0.15	2.88	
121	3.95	5.25	40.00	25.00	3.74	0.14	6.81	0.15	3.07	

122	3.55	6.00	47.50	25.00	3.66	0.32	4.07	0.67	0.41	
123	5.00	6.00	43.00	25.00	3.73	0.42	3.01	0.76	0.72	
124	4.30	6.00	34.00	25.00	2.42	0.10	4.58	0.67	2.16	
125	3.35	6.00	38.00	25.00	2.42	0.14	4.14	0.68	1.72	
126	4.00	5.30	40.50	25.00	3.87	0.16	6.81	0.18	2.93	
127	5.00	4.20	30.00	25.00	1.30	0.14	1.77	0.36	0.48	
128	3.95	5.20	40.00	25.00	3.61	0.13	6.78	0.12	3.18	
129	5.00	4.95	41.00	25.00	3.84	0.04	3.96	0.39	0.12	
130	3.95	5.30	40.00	25.00	3.63	0.11	6.81	0.18	3.19	
131	4.00	5.35	40.50	25.00	3.76	0.27	6.80	0.21	3.04	
132	3.00	6.00	30.00	25.00	3.88	0.65	1.77	0.74	2.11	
133	3.00	4.60	39.50	25.00	1.78	0.22	3.82	0.21	2.03	
134	5.00	5.75	30.00	25.00	1.26	0.12	2.07	0.55	0.82	
135	4.55	6.00	50.00	25.00	4.01	0.11	2.77	0.70	1.24	
136	4.05	5.25	40.50	25.00	3.94	0.27	6.78	0.15	2.84	
137	4.00	5.25	39.50	25.00	3.91	0.37	6.80	0.15	2.89	
138	3.95	5.25	40.50	25.00	3.83	0.29	6.80	0.15	2.97	
139	3.95	5.35	40.00	25.00	3.60	0.17	6.81	0.21	3.21	
140	3.05	4.00	30.00	25.00	1.16	0.13	1.88	0.04	0.72	
141	4.10	6.00	41.00	25.00	3.90	0.29	5.48	0.65	1.58	
142	3.70	4.90	44.00	25.00	3.71	0.22	5.87	0.18	2.17	
143	3.00	5.55	44.00	25.00	3.37	0.15	3.94	0.39	0.58	
144	4.30	4.00	50.00	25.00	2.97	0.10	2.59	0.32	0.39	
145	4.05	5.20	39.50	25.00	3.77	0.21	6.77	0.12	3.00	
146	3.95	5.30	40.50	25.00	3.61	0.09	6.80	0.18	3.20	
147	4.00	5.30	39.50	25.00	4.02	0.20	6.81	0.18	2.79	
148	5.00	4.00	43.00	25.00	3.01	0.34	3.02	0.27	0.01	
149	4.00	5.30	41.00	25.00	3.65	0.11	6.78	0.18	3.13	
150	4.75	5.75	45.00	25.00	3.74	0.25	1.26	1.28	2.48	
151	4.00	6.00	20.00	25.00	3.57	0.17	1.31	1.14	2.25	
152	4.00	6.00	30.00	25.00	3.48	0.17	2.08	0.40	1.40	
153	3.25	6.00	50.00	25.00	3.99	0.16	2.86	0.50	1.13	
154	3.75	4.25	50.00	25.00	3.28	0.13	0.58	1.36	2.70	
155	4.75	6.00	47.50	25.00	4.22	0.17	4.06	0.21	0.17	
156	3.00	6.00	50.00	25.00	4.05	0.06	2.33	0.64	1.73	
157	4.75	4.75	47.50	25.00	4.11	0.11	0.38	1.24	3.73	
158	4.25	6.00	47.50	25.00	4.12	0.13	4.33	0.20	0.21	
159	3.75	6.00	30.00	25.00	3.42	0.06	2.29	0.46	1.14	
160	3.75	6.00	50.00	25.00	3.77	0.30	3.76	0.33	0.01	
161	3.50	4.00	50.00	25.00	3.15	0.04	3.26	0.20	0.11	
162	5.00	6.00	45.00	25.00	4.06	0.15	3.73	0.34	0.33	
163	4.00	5.75	30.00	25.00	3.51	0.19	1.23	1.01	2.27	

Cycle 6

164	4.50	6.00	45.00	25.00	3.86	0.10	4.28	0.23	0.41	
165	3.50	6.00	50.00	25.00	3.63	0.15	3.35	0.40	0.28	
166	4.75	2.75	40.00	25.00	2.25	0.16	0.38	1.37	1.87	
167	4.00	4.00	20.00	25.00	3.24	0.45	0.56	0.86	2.68	
168	3.50	4.50	47.50	75.00	2.57	0.33	0.66	1.29	1.91	
169	3.00	6.00	50.00	75.00	2.50	0.28	1.69	1.06	0.81	
170	4.50	6.00	50.00	75.00	2.91	0.10	2.94	0.95	0.04	
171	3.75	4.50	47.50	75.00	2.79	0.51	0.58	1.31	2.21	
172	4.25	4.75	42.50	75.00	2.43	0.11	0.42	1.24	2.02	
173	4.00	6.00	20.00	75.00	1.84	0.05	0.96	1.26	0.89	
174	3.00	6.00	40.00	75.00	2.62	0.12	1.49	0.98	1.13	
175	3.50	2.00	40.00	75.00	1.21	0.31	1.96	0.94	0.75	
176	3.00	6.00	20.00	75.00	1.93	0.28	1.64	1.24	0.30	
177	3.25	6.00	45.00	75.00	2.98	0.63	2.01	0.98	0.97	
178	4.25	3.25	30.00	75.00	1.44	0.03	0.35	1.37	1.09	
179	3.75	2.50	50.00	75.00	1.36	0.15	0.00	1.38	1.35	
180	4.00	6.00	30.00	75.00	1.82	0.04	1.51	0.99	0.31	
181	3.50	6.00	40.00	75.00	2.61	0.25	2.06	0.96	0.56	
182	4.50	2.00	50.00	75.00	1.36	0.04	2.05	0.47	0.69	
183	2.00	6.00	40.00	75.00	1.92	0.35	0.64	1.25	1.28	
184	3.25	6.00	30.00	75.00	1.86	0.05	1.89	1.01	0.03	
185	4.00	5.25	45.00	75.00	2.56	0.14	2.65	0.98	0.09	

* Represents the anomalous experiment

***** No ML-predictions were made as this was the beginning experimental cycle.**

S8. References

(1) Rodrigues, F.; Ferru, G.; Berthon, L.; Boubals, N.; Guilbaud, P.; Sorel, C.; Diat, O.; Bauduin, P.; Simonin, J. P.; Morel, J. P.; Morel-Desrosiers, N.; Charbonnel, M. C. New insights into the extraction of uranium(VI) by an N,N-dialkylamide. *Molecular Physics* **2014**, *112* (9-10), 1362-1374. DOI: 10.1080/00268976.2014.902139.

(2) Pathak, P. N.; Kumbhare, L. B.; Manchanda, V. K. STRUCTURAL EFFECTS IN N,N-DIALKYL AMIDES ON THEIR EXTRACTION BEHAVIOR TOWARD URANIUM AND THORIUM. *Solvent Extraction and Ion Exchange* **2001**, *19* (1), 105-126. DOI: 10.1081/SEI-100001377.

(3) Pathak, P. N.; Veeraraghavan, R.; Prabhu, D. R.; Mahajan, G. R.; Manchanda, V. K. Separation Studies of Uranium and Thorium Using Di-2-Ethylhexyl Isobutyramide (D2EHIBA). *Separation Science and Technology* **1999**, *34* (13), 2601-2614. DOI: 10.1081/SS-100100793.

(4) Prabhu, D. R.; Mahajan, G. R.; Nair, G. M. Di(2-ethyl hexyl) butyramide and di(2-ethyl hexyl)isobutyramide as extractants for uranium(VI) and plutonium(IV). *Journal of Radioanalytical and Nuclear Chemistry* **1997**, *224* (1), 113-117. DOI: 10.1007/BF02034622.

(5) Condamines, N.; Musikas, C. THE EXTRACTION BY N.N-DIALKYLAMIDES. II. EXTRACTION OF ACTINIDE CATIONS. *Solvent Extraction and Ion Exchange* **1992**, *10* (1), 69-100. DOI: 10.1080/07366299208918093.

(6) Pathak, P. N.; Veeraraghavan, R.; Ruikar, P. B.; Manchanda, V. K. Solvent Extraction Studies on Th(IV), Pa(V) and U(VI) from Nitric Acid Medium using Di-2-Ethyl Hexyl Isobutyramide (D2EHIBA). *Radiochimica Acta* **1999**, *86* (3-4), 129-134. DOI: 10.1524/ract.1999.86.34.129.

(7) Hall, G. B.; Campbell, E. L.; Bessen, N. P.; Graham, T. R.; Cho, H.; RisenHuber, M.; Heller, F. D.; Lumetta, G. J. Extraction of Nitric Acid and Uranium with DEHiBA under High Loading Conditions. *Inorganic Chemistry* **2023**, *62* (17), 6711-6721. DOI: 10.1021/acs.inorgchem.3c00288.

(8) Hall, G. B.; Bessen, N. P.; Zalupski, P. R.; Campbell, E. L.; Grimes, T. S.; Peterman, D. R.; Lumetta, G. J. Extraction of Neptunium, Plutonium, Americium, Zirconium, and Technetium by Di-(2-Ethylhexyl)-Iso-Butyramide (DEHiBA) at High Metal Loadings. *Solvent Extraction and Ion Exchange* **2023**, *41* (5), 545-563. DOI: 10.1080/07366299.2023.2215833.

(9) McCann, K.; Mincher, B. J.; Schmitt, N. C.; Braley, J. C. Hexavalent Actinide Extraction Using N,N-Dialkyl Amides. *Industrial & Engineering Chemistry Research* **2017**, *56* (22), 6515-6519. DOI: 10.1021/acs.iecr.7b01181.

(10) Manchanda, V. K.; Ruikar, P. B.; Sriram, S.; Nagar, M. S.; Pathak, P. N.; Gupta, K. K.; Singh, R. K.; Chitnis, R. R.; Dhami, P. S.; Ramanujam, A. Distribution Behavior of U(VI), Pu(IV), Am(III), and Zr(IV) with N,N-Dihexyl Octanamide under Uranium-Loading Conditions. *Nuclear Technology* **2001**, *134* (3), 231-240. DOI: 10.13182/NT01-A3198.

(11) Mowafy, E. A.; Aly, H. F. EXTRACTION OF ACTINIDES AND SELECTED FISSION PRODUCTS FROM NITRIC ACID MEDIUM USING LONG CHAIN MONOAMIDES. *Solvent Extraction and Ion Exchange* **2001**, *19* (4), 629-641. DOI: 10.1081/SEI-100103812.

(12) Gupta, K. K.; Manchanda, V. K.; Subramanian, M. S.; Singh, R. K. SOLVENT EXTRACTION STUDIES ON U(VI), Pu(IV), AND FISSION PRODUCTS USING N,N-DIHEXYLOCTANAMIDE. *Solvent Extraction and Ion Exchange* **2000**, *18* (2), 273-292. DOI: 10.1080/07366290008934681.

(13) Pathak, P. N.; Kumbhare, L. B.; Manchanda, V. K. Effect of structure of N,N dialkyl amides on the extraction of U(VI) and Th(IV): a thermodynamic study. *Radiochimica Acta* **2001**, *89* (7), 447-452. DOI: 10.1524/ract.2001.89.7.447.

(14) Gupta, K. K.; Manchanda, V. K.; Subramanian, M. S.; Singh, R. K. N,N-Dihexyl Hexanamide: A Promising Extractant for Nuclear Fuel Reprocessing. *Separation Science and Technology* **2000**, *35* (10), 1603-1617. DOI: 10.1081/SS-100100243.
(15) Gupta, K. K.; Manchanda, V. K.; Subramanian, M. S.; Singh, R. K. Thermodynamics of Extraction of Uranium(VI) and Plutonium(IV) with some Long-chain Aliphatic Amides. *Radiochimica Acta* **1999**, *85* (3-4), 103-106. DOI: 10.1524/ract.1999.85.34.103.
(16) Nair, G. M.; Prabhu, D. R.; Mahajan, G. R. Extraction of uranium(VI) and plutonium(IV) with dihexylbutyramide and dihexylisobutyramide from nitric acid medium. *Journal of Radioanalytical and Nuclear Chemistry* **1994**, *182* (2), 393-399. DOI: 10.1007/BF02037516.
(17) Nair, G. M.; Mahajan, G. R.; Prabhu, D. R. Dioctyl butyramide and dioctyl isobutyramide as extractants for uranium(VI) and plutonium(IV). *Journal of Radioanalytical and Nuclear Chemistry* **1996**, *204* (1), 103-111. DOI: 10.1007/BF02060871.
(18) Siddall, T. H., III. EFFECTS OF STRUCTURE OF N,N-DISUBSTITUTED AMIDES ON THEIR EXTRACTION OF ACTINIDE AND ZIRCONIUM NITRATES AND OF NITRIC ACID1. *The Journal of Physical Chemistry* **1960**, *64* (12), 1863-1866. DOI: 10.1021/j100841a014.
(19) Suzuki, S.; Sasaki, Y.; Yaita, T.; Kimura, T. *Study on selective separation of uranium by N,N-dialkyl-amide in ARTIST process*; INIS-FR--2929; France, 2004. http://inis.iaea.org/search/search.aspx?orig_q=RN:36010983.
(20) Sun, G.-X.; Han, J.-T.; Bao, B.-R.; Sun, S.-X. Structural effect of N,N-dialkylamide in toluene on the extraction of uranium(VI). *Journal of Radioanalytical and Nuclear Chemistry* **1998**, *232* (1), 245-247. DOI: 10.1007/BF02383748.
(21) Ardois, C.; Mokili, M. B.; Musikas, C.; Abbé, J. C. The use of the N,N-diethyldodecanamide for actinide extraction in conjunction with liquid scintillation counting. *Journal of Radioanalytical and Nuclear Chemistry* **1999**, *240* (3), 751-761. DOI: 10.1007/BF02349849.
(22) Pathak, P. N.; Prabhu, D. R.; Ruikar, P. B.; Mancha, V. K. EVALUATION OF DI(2-ETHYLHEXYL)ISOBUTYRAMIDE (D2EHIBA) AS A PROCESS EXTRACTANT FOR THE RECOVERY OF 233U FROM IRRADIATED Th. *Solvent Extraction and Ion Exchange* **2002**, *20* (3), 293-311. DOI: 10.1081/SEI-120004806.
(23) Pathak, P. N.; Prabhu, D. R.; Manchanda, V. K. The role of oxidants in Pu-Th separation studies employing di(2-ethylhexyl)isobutyramide (D2EHIBA) as extractant. *Radiochimica Acta* **2003**, *91* (3), 141-146. DOI: 10.1524/ract.91.3.141.19979.
(24) Pathak, P. N.; Prabhu, D. R.; Rizvi, G. H.; Ruikar, P. B.; Kumbhare, L. B.; Mohapatra, P. K.; Manchanda, V. K. Pu-Th separation studies employing di(2-ethylhexyl)isobutyramide (D2EHIBA) as extractant from nitric acid medium. *Radiochimica Acta* **2003**, *91* (7), 379-384. DOI: 10.1524/ract.91.7.379.20012.
(25) Manchanda, V. K.; Pathak, P. N.; Rao, A. K. Di(2-Ethylhexyl) Pivalamide (D2EHPVA): A Promising Extractant for Selective Removal of Uranium from High Level Nuclear Waste Solutions. *Solvent Extraction and Ion Exchange* **2004**, *22* (3), 353-375. DOI: 10.1081/SEI-120030396.
(26) Musikas, C. Potentiality of Nonorganophosphorus Extractant in Chemical Separations of Actinides. *Separation Science and Technology* **1988**, *23* (12-13), 1211-1226. DOI: 10.1080/01496398808075626.
(27) Pathak, P. N.; Prabhu, D. R.; Kanekar, A. S.; Manchanda, V. K. Recent R&D Studies Related to Coprocessing of Spent Nuclear Fuel Using N,N-Dihexyloctanamide. *Separation Science and Technology* **2009**, *44* (15), 3650-3663. DOI: 10.1080/01496390903183147.

(28) Pathak, P. N.; Prabhu, D. R.; Kanekar, A. S.; Manchanda, V. K. Evaluation of N,N-dialkylamides as promising process extractants. *IOP Conference Series: Materials Science and Engineering* **2010**, *9* (1), 012082. DOI: 10.1088/1757-899X/9/1/012082.
(29) Gasparini, G. M.; Grossi, G. Application of N, N-Dialkyl Aliphatic amides in the Separation of Some Actinides. *Separation Science and Technology* **1980**, *15* (4), 825-844. DOI: 10.1080/01496398008076273.
(30) Nair, G. M.; Mahajan, G. R.; Prabhu, D. R. Extraction of uranium(VI) and plutonium(IV) with some high molecular weight aliphatic monoamides from nitric acid medium. *Journal of Radioanalytical and Nuclear Chemistry* **1995**, *191* (2), 323-330. DOI: 10.1007/BF02038228.
(31) Mahanty, B.; Kanekar, A. S.; Ansari, S. A.; Bhattacharyya, A.; Mohapatra, P. K. Separation of neptunium from actinides by monoamides: a solvent extraction study. *Radiochimica Acta* **2019**, *107* (5), 369-376. DOI: 10.1515/ract-2018-3074.
(32) Horne, G. P.; Zarzana, C. A.; Grimes, T. S.; Rae, C.; Ceder, J.; Mezyk, S. P.; Mincher, B. J.; Charbonnel, M.-C.; Guilbaud, P.; Saint-Louis, G.; Berthon, L. Effect of chemical environment on the radiation chemistry of N,N-di-(2-ethylhexyl)butyramide (DEHBA) and plutonium retention. *Dalton Transactions* **2019**, *48* (38), 14450-14460. DOI: 10.1039/C9DT02383F.
(33) Gogolski, J. M.; Jensen, M. P. Using N,N-dialkylamides for neptunium purification from other actinides for space applications. *Separation Science and Technology* **2021**, *56* (16), 2775-2788. DOI: 10.1080/01496395.2020.1845209.
(34) Noack, M. M.; Doerk, G. S.; Li, R.; Streit, J. K.; Vaia, R. A.; Yager, K. G.; Fukuto, M. Autonomous materials discovery driven by Gaussian process regression with inhomogeneous measurement noise and anisotropic kernels. *Scientific Reports* **2020**, *10* (1), 17663. DOI: 10.1038/s41598-020-74394-1.
(35) Rasmussen, C. E.; Williams, C. K. I. *Gaussian Processes for Machine Learning*; the MIT Press, 2006.
(36) Ginsbourger, D.; Le Riche, R.; Carraro, L. Kriging Is Well-Suited to Parallelize Optimization. In *Computational Intelligence in Expensive Optimization Problems*, Tenne, Y., Goh, C.-K. Eds.; Springer Berlin Heidelberg, 2010; pp 131-162.
(37) Ginsbourger, D.; Le Riche, R.; Carraro, L. A Multi-points Criterion for Deterministic Parallel Global Optimization based on Gaussian Processes. **2008**.
(38) Schonlau, M. Computer experiments and global optimization. University of Waterloo, 1997.
(39) Hernández-Lobato, J. M.; Requeima, J.; Pyzer-Knapp, E. O.; Aspuru-Guzik, A. Parallel and distributed Thompson sampling for large-scale accelerated exploration of chemical space. In *International conference on machine learning*, 2017; PMLR: pp 1470-1479.
(40) Kandasamy, K.; Krishnamurthy, A.; Schneider, J.; Póczos, B. Parallelised Bayesian optimisation via Thompson sampling. In *International Conference on Artificial Intelligence and Statistics*, 2018; PMLR: pp 133-142.
(41) Nguyen, V.; Gupta, S.; Rana, S.; Li, C.; Venkatesh, S. Practical batch bayesian optimization for less expensive functions. *arXiv preprint arXiv:1811.01466* **2018**.
(42) Shields, B. J.; Stevens, J.; Li, J.; Parasram, M.; Damani, F.; Alvarado, J. I. M.; Janey, J. M.; Adams, R. P.; Doyle, A. G. Bayesian reaction optimization as a tool for chemical synthesis. *Nature* **2021**, *590* (7844), 89-96. DOI: 10.1038/s41586-021-03213-y.